Experimental and Theoretical Insights into the Optical Properties and Intermolecular Interactions in Push-Pull Bromide Salts

Perumal Venkatesan,[a] Margarita Cerón,[a] Enrique Pérez-Gutiérrez,[a] Armando E. Castillo,[a] Subbiah Thamotharan,[b] Fernando Robles,[c] Maxime A. Siegler,[d] and M. Judith Percino*[a]

Experimental and theoretical insights into the nature of intermolecular interactions and their effect on optical properties of 1-allyl-4-(1-cyano-2-(4-dialkylaminophenyl)vinyl)pyridin-1-ium bromide salts (I and II) are reported. A comparison of optical properties in solution and in the solid-state of the salts (I and II) with their precursors (Ia and IIa) is made. The experimental absorption maxima (λ_{max}) in CHCl$_3$ is at 528 nm for I and at 542 nm for II, and a strong bathochromic shift of ~110 nm is observed for salts I and II compared with their precursors. The absorption bands in solid-state at ~627 nm for I and at ~615 nm for II that are assigned to charge transfer (CT) effect. The optical properties and single crystal structural features of I and II are explored by experimental and computational tools.

The calculated λ_{max} and the CT are in good agreement with the experimental results. The intermolecular interactions existing in the crystal structures and their energies are quantified for various dimers by PIXEL, QTAIM and DFT approaches. Three types of interactions, (i) the cation⋯cation interactions, (ii) cation⋯anion interactions and (iii) anion⋯anion interactions are observed. The cationic moiety is mainly destabilized by C−H⋯N/π and π⋯π interactions whereas the cation and anion moiety is predominantly stabilized by strong C−H⋯Br$^-$ interactions in both structures. The existence of charge transfer between cation and anion moieties in these structures is established through NBO analysis.

1. Introduction

Fluorescence dyes are widely used as fluorescence probes which are used in the chemistry, biology and physics for monitoring specific properties such as ON-OFF switches, ion sensing, explosive detection, luminescence-based bioimaging,[1] etc. Luminescence property of the materials is sensitive to the external stimuli such as temperature, polarity, viscosity, pH and crystal packing.[2] On the other hand, fluorescence probes based on the stilbazolium salts (D-π-A$^+$X$^-$) are used to monitor viscosity, pH,[3] and photopolymerization reaction of methyl

acrylates[4] and other polymerization processes.[5] The photophysical and spectroscopy studies on the quaternary salt (D-π-A$^+$ X$^-$) have been reported by Fromherz's[6] and Rettig's[7] research groups. Recently, Yu, et al. reported a (Z)-4-(4-(1-cyano-2-(4-dimethylamino)phenyl)vinyl)phenyl)-1-methylpyridin-1-ium hexafluorophosphate quaternary salt (Scheme 1, a), which is used as a luminescent imaging agent for mitochondria and nucleolus in living cells. The salt exhibits two different color emission in the mitochondria and cell nucleolus.[8] The (Z)-4-(4-(1-cyano-2-(4-diphenylamino)phenyl)vinyl)phenyl)-1-methylpyridin-1-ium hexafluorophosphate, (Scheme 1, b) has been reported as mitochondrion-targeted photosensitizing agents for the visualization of cancer cells.[9]

Last few decades, an impressive amount of attention has been devoted to the development of various organic D-π-A systems, because they have high polarizability and the strong intramolecular charge transfer (ICT) abilities. A typical push-pull organic D-π-A chromophore consists of strong electron donors (D) and acceptors (A) which are interlinked by a π-conjugated system. The intramolecular charge transfer (ICT) between donor

[a] Dr. P. Venkatesan, Dr. M. Cerón, Dr. E. Pérez-Gutiérrez, A. E. Castillo, Prof. M. J. Percino
Unidad de Polímeros y Electrónica Orgánica, Instituto de Ciencias, Benemérita Universidad Autónoma de Puebla, Val3-Ecocampus Valsequillo, Independencia O2 Sur 50, San Pedro Zacachimalpa, Pue, México
E-mail: judith.percino@correo.buap.mx

[b] Dr. S. Thamotharan
Biomolecular Crystallography Laboratory, Department of Bioinfor- matics, School of Chemical and Biotechnology, SASTRA Deemed University, Thanjavur 613 401, India

[c] F. Robles
Laboratorio Nacional del Sureste de México, BUAP, Blvd., Valsequillo S/N esquina Blvd. Municipio Libre, C.P. 72500 Puebla, México
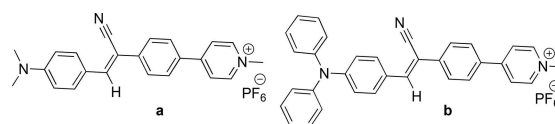
[d] Dr. M. A. Siegler
Department of Chemistry, Johns Hopkins University, New Chemistry Building, 3400N.Charles St. Baltimore, MD, 21218, USA

Scheme 1. The chemical diagram of (Z)-4-(4-(1-cyano-2-(4-dimethylamino) phenyl)vinyl)phenyl)-1-methylpyridin-1-ium hexafluorophosphate[8] (a) and (Z)-4-(4-(1-cyano-2-(4-(diphenylamino)phenyl)vinyl)phenyl)-1-methyl-pyridin-1-ium hexafluorophosphate[9] (b).

and acceptor moieties in D-π-A molecules is well studied.[10] In general, the characteristic of the push-pull properties on the D-π-A chromophore is mainly depending on the electronic behavior of donors and acceptors moieties and also on the length of the π-conjugated linker.[11] The strong electron-donor substituents (N,N-dialkyl or arylamino (—NPh₂) or alkoxy (—OR)) and strong electron-withdrawing moieties (nitro (—NO₂) or cyano (—CN)) are used to construct the D-π-A systems with low band gap and an intense ICT property. Various π-conjugated bridges, including triple or double bonds,[10a,c, 12] aromatics[13] and heteroaromatics,[13d,14] have been used as a π-linker for D-π-A chromophore. Moreover, the band gap and the ICT property of D-π-A molecules can be tuned by changing the donor, acceptor and π-linkers.[15] Ethylene molecules with strong electron-donor and acceptor moieties come also under the category of D-π-A family. The breaking of the C=C bond is rarely observed at the normal condition in the substituted push-pull molecules which contain one donor and one acceptor (HDC=CAH). However, conversion of the zwitterionic form (Scheme 2, **b**) in the push-pull molecule DD′C=CAA′(Scheme 2, **a**) with strong D and an acceptor A group has been experimentally confirmed.[16]

Scheme 2. The push-pull ethylene molecule.[16]

The formation of the zwitterionic form (Scheme 2, **b**) is enhanced by a strong polarization of the molecule due to strong π-electron delocalization between donor and acceptor groups. Because, the electronic perturbation nature of donor and acceptor can enhance the π-electron delocalization on the molecular structure, and it is also reflected on bond lengths as well. The strong π-electron delocalization can significantly be weakened the C=C bond character, and it reduces the electron density around the C=C bond. As a result, the rotation of C=C bond in this class of compounds was observed. The steric factor of substituents (D and A), also plays a crucial role in twisting and elongating the central C=C bond.

Recently, our group has been explored the Z→E transformation of **Ia**, (Z)-3-[4-(dimethylamino)phenyl]-2-(4-pyridyl) prop-2-enenitrile under different solvent environment, and the Z/E ratio was determined by using ¹H-NMR spectroscopy at room temperature.[17] The weakening of the C=C bond character influenced by the solvent effect helps to undergo Z/E transformation. Several studies have explained the structure-property relationship specifically the optical properties of different (Z)-3-substituted phenyl-2-(phenyl/pyridyl)acrylonitrile derivatives (which are belongs to D-π-A system) with different D and A groups.[18]

In this study, we compared the optical and charge transfer properties of the precursors (Scheme 3, (Z)-3-[4-(dimethylamino)phenyl]-2-(4-pyridyl)prop-2-enenitrile(**Ia**) and (Z)-3-[4-(diphenylamino)phenyl]-2-(4-pyridyl)prop-2-enenitrile (**Ib**)) with title

salts **I** and **II** (1-allyl-4-(1-cyano-2-(4-(dimethylamino) phenyl) vinyl)pyridin-1-ium bromide (**I**); 1-allyl-4-(1-cyano-2-(4-(diphenylamino)phenyl)vinyl)pyridin-1-ium bromide (**II**), (see Scheme 4).
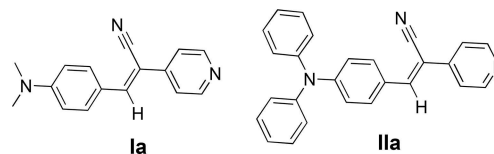
Scheme 3. Chemical diagram for precursor compounds (Z)-3-[4-(dimethylamino)phenyl]-2-(4-pyridyl)prop-2-enenitrile (**Ia**) and (Z)-3-[4-(diphenylamino) phenyl]-2-(4-pyridyl)prop-2-enenitrile (**IIa**).
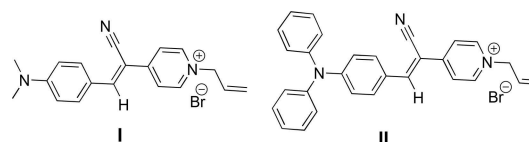
Scheme 4. Chemical diagram of (Z)-1-allyl-4-(1-cyano-2-(4-(dimethylamino) phenyl)vinyl)pyridin-1-ium bromide(**I**) and (Z)-1-allyl-4-(1-cyano-2-(4-(diphenylamino)phenyl)vinyl)pyridin-1-ium bromide (**II**).

2. Results and Discussion

In this study, we explored the effect of quarternization on the pyridine nitrogen atom in **I–II** in comparison with their precursor compounds (**Ia–IIa**), in terms of (i) the push-pull characters, (ii) absorption properties, (iii) the intra- and inter-molecular charge transfers (ICT) properties, as well as (iv) intermolecular interactions in the crystalline state. Both salts were obtained from the quaternization reaction of respective precursor compounds (**Ia–IIa**) with allyl bromide (**3**) (Scheme 5) by using the synthesis procedures which reported for different alkylaminopyridinium bromide salts.[38] The synthesized salts were characterized by IR, NMR and mass spectrometry.
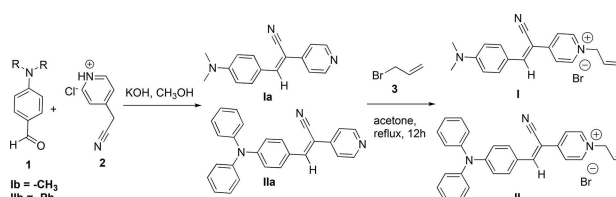
Scheme 5. Synthesis of salts **I–II** and **Ia–IIa**.

Single Crystal X-Ray Crystallography

Both salts (**I–II**) crystallize in the monoclinic crystal system with space groups P2₁/n for **I** and P2₁/c for **II**. Crystallographic data and refinement statistics are presented in Table 1. The ORTEP

Table 1. Crystal data and refinement parameters for I–II.

Parameters	I	II
Empirical formula	$C_{19}H_{20}N_3{}^+$, Br$^-$	$C_{29}H_{24}N_3{}^+$, Br$^-$
Color, Morphology	dark red, block	red, thick plate
Formula weight	370.29	494.42
T(K)	110	110
Wavelength (Å)	1.54178	0.71073
Crystal system	Monoclinic	Monoclinic
Space group	$P2_1/n$	$P2_1/c$
a (Å)	7.45974(14)	18.8430 (5)
b (Å)	24.9280(4)	13.1737 (4)
c (Å)	9.66801(19)	9.7074 (3)
α (°)	90.00	90.00
β (°)	106.020(2)	95.804 (2)
γ (°)	90.00	90.00
V (Å^3)	1728.01(6)	2397.33 (12)
Z	4	4
Dx (g/m^3)	1.423	1.370
μ (mm^{-1})	3.25	1.74
F (000)	760	1016
Crystal size (mm)	$0.21 \times 0.17 \times 0.15$	$0.40 \times 0.27 \times 0.08$
No. of measured, independent and observed [$I > 2\sigma(I)$] reflections	11417, 3378, 3001	32066, 5517, 4826
R1 [$I > 2\sigma(I)$], R1 [all]	0.0271, 0.0317	0.0264, 0.0341
wR2 [$I > 2\sigma(I)$], wR2 [all]	0.0694, 0.0722	0.0638, 0.671
Goodness-of-fit	1.043	1.040
Largest difference in peak and hole (e Å^{-3})	0.310 and −0.374	0.36 and −0.34
CCDC number	1863461	1863462

Table 2. The selected torsion angle in I–II and Ia–IIa (θ, °).

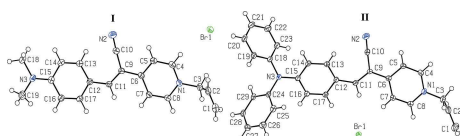| Atoms	Compounds			
	I	Ia	II	IIa
C5–C6–C9–C11	−176.0(2)	−178.4(1)	171.9(2)	−145.6(2)
C7–C6–C9–C10	−176.8(2)	−177.5(1)	171.5(2)	−151.6(2)
C9–C11–C12–C13	−5.7(4)	−7.0(2)	−7.5(3)	20.5(3)
C9–C11–C12–C17	174.1(2)	174.0(1)	175.5(2)	−161.3(2)
C14–C15–N3–C18	5.6(3)	2.4(2)	37.6(2)	31.9(2)
C14–C15–N3–C19/C24	−176.8(2)	−173.8(1)	−148.4(2)	−149.6(1)
C16–C15–N3–C18	−174.6(2)	−178.2(1)	−143.0(2)	−148.6(1)
C16–C15–N3–C19/C24	3.1(3)	5.6(2)	31.1(2)	30.0(2)
C1–C2–C3–N1	115.5(2)		−129.6(2)	
C2–C3–N1–C4	111.0(2)		−125.3(2)	
C2–C3–N1–C8	−66.1(2)		57.1(2)	

Figure 1. Displacement ellipsoidal plots (at the 50% probability level) of I–II with atom-numbering scheme.
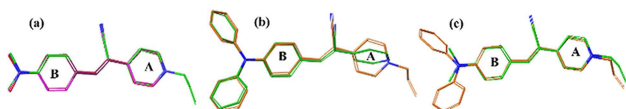

Figure 2. (a) Overlay of I (green) and Ia (molecule A in form I:purple; molecule B in form I:magenta and molecule in form II:red); (b) overlay of II and IIa; (c) overlay of I and II (The cationic moiety of I (green) and II(orange) is only used for structural superimposition).

diagram shows the asymmetric units of I–II along with the atom-numbering scheme (Figure 1). In both salts, the stoichiometry between cation and anion is 1:1.

The salts I and II consist of either electron donor group 4-(N,N-dimethylamino)phenyl, or 4-(N,N-diphenylamino)phenyl moiety attached to double bond and electron acceptor group (nitrile moiety and the quaternary pyridinium ring) labelled as **4Py$^+$ECN**. In the case of the free base, the electron acceptor group is marked as **4PyECN** (Ia–IIa, Scheme 3). Compound **Ia** crystallized in two different forms (triclinic $P\bar{1}$ space group; refcode: TENMIK, polymorph-1[18e] and monoclinic $P2_1/c$ space group; refcode: TENMIK01, polymorph-2).[18d] The asymmetric unit of polymorph-1 contains two crystallographically independent molecules, whereas, polymorph-2 contains one mole-

cule in the asymmetric unit. Compound **IIa** crystallized in the orthorhombic *Pbcn* space group (refcode: AWEGEQ) with one molecule in the asymmetric unit.[18b] In order to understand the effect of quaternization of the pyridine nitrogen atom in I–II, a detailed structural comparison of I–II and their precursor structures (Ia–IIa)[18b,d,e] has been performed. As shown in Figure 2(a), the structure of I is well overlaid with both forms of Ia. Superimposition of II and IIa shows that the quarternized pyridine (ring A) is rotated. In the cases of I and II, the N,N-dimethyl or N, N-diphenyl is slightly rotated and we found that the allyl group exhibits different conformations in these structures (Figure 2(c)). The selected torsion angles clearly show the pyridine ring rotation in II (Figure 2 and Table 2). The bond lengths and torsion angles of I–II and their precursor compounds (Ia–IIa) are summarized in Tables S1–S4, ESI.

To understand the push-pull effect due to the salt formation, I–II, i.e., how the push-pull character is enhanced by the quaternization of pyridine nitrogen when it is compared to their precursor compounds. This comparison is expressed in terms of bond length variation, absorption, charge transfer properties and energy level difference in the frontier molecular orbitals. From Tables S1 and S3, the bond length of C9=C11 is 1.372(3) Å in I which is slightly elongated as compared to the corresponding bond length in II (1.357(2) Å). In the precursor, the corresponding bond length is found to be shorter (1.358(2) Å in Ia and 1.348(2) Å in IIa, see Figures S1–S2). Similar elongation of Csp^2=Csp^2 bond length was observed in conjugated ethylene's molecules in the range of 1.331(9)–1.392(17) Å. Similarly, the bond length of C12–C11 is 1.429(3) Å in I and 1.445(2) Å in II being shorter than those of their precursor structures (1.441(2) in Ia and 1.454(2) in IIa). It is to be noted that bond length shortening is also observed for C6–C9 bond length (1.457 (3) Å in I; 1.468(2) Å in II and 1.481(2) Å in Ia and 1.487(2) Å in IIa). The shortening and elongation of bonds in the central part of the structures I–II (Figures S1-S2, acrylonitrile group) suggest that the whole molecule participates in the electronic delocalization. The strong conjugation and push-pull characteristic of I–II are mainly due to the stronger electron pulling (−I effect) nature of **4Py$^+$ECN** cation as compared to neutral **4PyECN** model found in Ia–IIa. This indicates that the electron withdrawing (−I effect) nature of **4Py$^+$ECN** cation in I–II is stronger as compared to the **4PyECN** in Ia–IIa.
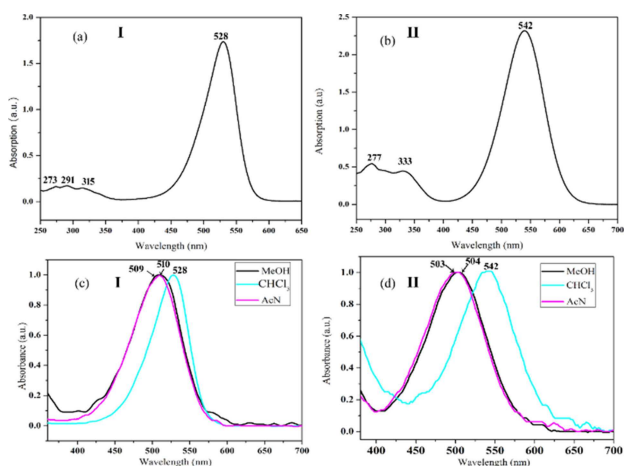
Figure 3. Absorbance spectra of **I (a)** and **II (b)** in CHCl₃. Absorbance spectra of **I (c)** and **II (d)** in polar solvent and CHCl₃.

Figure 4. Solutions of the salts **I** and **II** in different solvents and UV spectra of them.

Optical Characterization

Absorption Properties in Solution

The effect of quaternization on the nitrogen atom of pyridine ring in **I** and **II** is reflected in the absorption properties when compared to their precursor compounds **Ia** and **IIa**. To understand this, we recorded the absorption spectra for **I** and **II** in different solvents (CHCl₃, CH₃OH, EtOH and CH₃CN), and in the solid-state. The absorption maxima (λ_{max}) for **I** is found at 528 nm in CHCl₃ along with three weak absorption peaks at 315, 291 and 273 nm (Figure 3(a)). For **II**, λ_{max} is observed at 542 nm and two weak absorptions at 333 and 277 nm in CHCl₃ (Figure 3(b)). The λ_{max} is slightly red-shifted (by 14 nm) in the case of **II**. In both **I** and **II**, the absorption of higher intensity is assigned to S₀→S₁ transition (π→π*), while the weak absorption corresponds to n→π* transition. For comparison, we also acquired the absorption spectra of **Ia** and **IIa** in CHCl₃. The λ_{max} at 422 nm for **Ia** and at 427 nm for **IIa** and these values are very similar with reported values.[18d]

The results show a strong bathochromic shift in the range of 106–115 nm on the absorption λ_{max} in CHCl₃ for **I** and **II** compared to their precursor compounds, **Ia** and **IIa**, (Tables 2 and S5). This strong bathochromic shift in **I–II** is an indication of push-pull effect induced by strong electron withdrawing of **4Py⁺ECN** cation. The positively charged **4Py⁺ECN** strongly attract the electrons from the electron rich bromide ion (**Br⁻**) and donor (D). As a result, the push-pull character clearly affects the bond lengths as mentioned above. Moreover, the intermolecular charge transfer (ICT) could arise from the interactions between molecular dipoles and the shifting of electron density of the donor due to the strong pulling of electrons observed earlier.[39]

Furthermore, to understand the solvatochromism properties of salts **I–II**, we recorded the absorption spectra in CHCl₃, CH₃OH and CH₃CN (Figure 3, (c) and (d)). It can be seen that the absorption peak is nearly the same in protic (CH₃OH) and aprotic (CH₃CN) solvents. Moreover, there is a negative
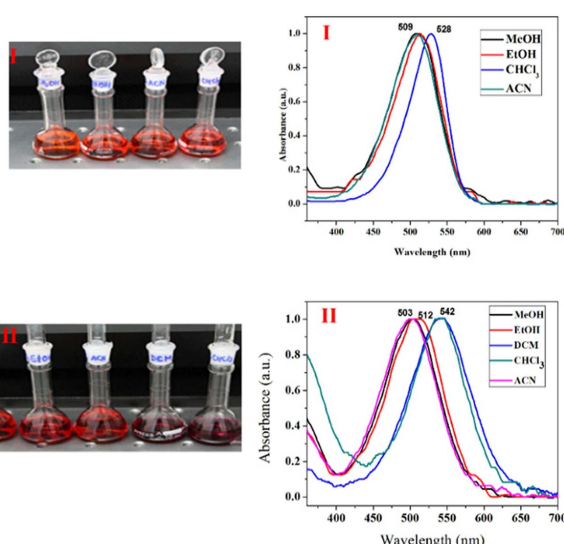
solvatochromism (blue shift; 19–30 nm) observed when increasing the polarity of the solvent. A similar trend is observed in other salts reported earlier.[39a,b,d,40] The longer λ_{max} of salts **I–II** in CHCl₃ could be due to the ion-pairs formation in CHCl₃. The similar ion-pairs formation existing in styrylpyridinium iodide in low polar solvents (THF, CHCl₃ and DCM ($E_T^N < 0.3$)), and its CT absorption characters due to photoinduced electron transfer from iodide to excited singlet state of the cation (styrylpyridinium).[41] In another study, the free ions of stilbazolium salts were found in highly polar solvents ($E_T^N > 0.4$) and present as ion-pair (contact pairs) in low polar solvents ($0.15 < E_T^N > 0.3$).[42] Figure 4 shows the solutions of salts **I** and **II** in different solvents. The purple color solution (**I–II** in CHCl₃/DCM) is an indication of strong interactions between cations and anions. The reason for the color change (the orange-red color solution in EtOH/MeOH/ACN) might be due to free ions present in the solution, *i.e.*, less interaction between cation and anion.

Dipole Moment

To understand the formation of ion pair in solution, the dipole moment (μ) was calculated by DFT method (Table 3). It can be seen from Table 3, in all three solvents, the μ value is higher in the case of salts **I** and **II**, whereas the corresponding value is lower for the precursor compounds **Ia** and **IIa**. The dipole

Table 3. The calculated dipole moment (μ) value in Debye. (at the B3LYP/6-311++G(d, p) level of theory).

Solvent	Compound			
	I	Ia	II	IIa
Chloroform	23.06	11.71	21.28	9.54
Methanol	25.12	12.83	22.73	10.41
Acetonitrile	23.89	12.84	22.75	10.42
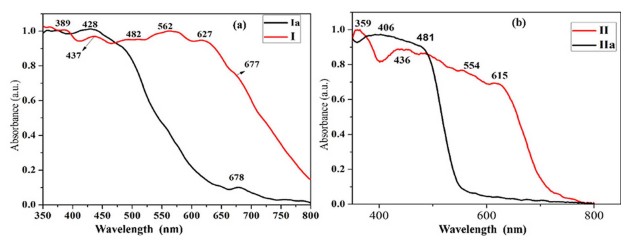
Figure 5. Absorbance spectra of **I** and **Ia** in the solid-state (**a**). Absorbance spectra of **II** and **IIa** in the solid-state (**b**).

moment is increased when quaternization occurs. We also noted that the differences in the dipole moment in different solvents could be the reason for color changes.

Absorption Properties in the Solid-state

The solid-state absorption spectra of **I–Ia** and **II–IIa** are shown in Figure 5 (a) and (b), respectively. The solid-state absorption spectra of **I–II** are very broad compared to **Ia** and **IIa**. A strong bathochromic shift of ~150 to 200 nm is observed for **I** and **II** when compared to **Ia** and **IIa**. This difference is clearly indicating the involvement of allyl moiety in the intermolecular interactions and the presence of interactions between cation and anion in both **I** and **II**. Moreover, the interactions are weaker in the solution and thereby weak bathochromic shift (~50 to 100 nm). The λ_{max} at ~627 nm for **I** and 615 nm for **II** is observed in the solid-state which indicates the presence strong CT between cation and anion in both compounds. It is noted that the very broad absorption peaks in the range of 420–680 nm are observed in **I–II**, whereas they are not observed in **Ia–IIa** which in turn supports for the existence of cation and anion interactions in **I–II**.

The morphology and color of crystals **I–II** were recorded using an optical microscope under normal light (Figure 6). The graining powder materials of **I–II** is in the dark brown color, whereas the single crystals of **I–II** existing in the metallic bright brown color. The metallic brightness was lost when grinding the crystal to powder. The precursor compounds (**Ia–IIa**) exhibit
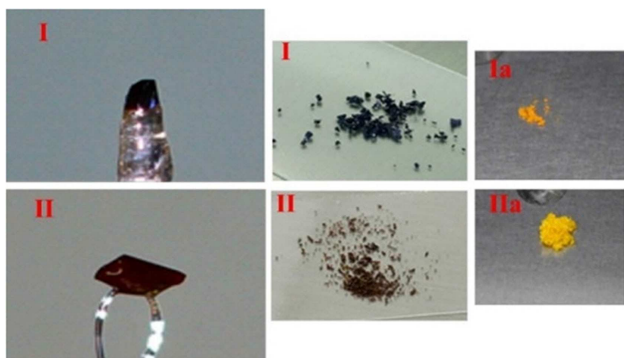
an orange-yellow color and there is no significant color change when crystals were grained to powder.

Theoretical Calculation on Absorption Properties

The electronic transitions of **I–II** were computed by TD-DFT method in the gas phase, in a solution state (CHCl$_3$, CH$_3$OH and CH$_3$CN); and in solid-state (crystal structure geometry), with B3LYP/6-311++G (d, p) level of theory. The calculated absorption wavelength (λ_{abs}), oscillator strengths (f), and major orbital transitions (in %) for **I–II** are compared with their respective precursor compounds (**Ia–IIa**) (Table 4 and Table S5, ESI). The most important molecular orbitals (HOMO and LUMO) transitions are presented in Figure 7. From Table 4, the computed absorption peaks above 600 nm in both **I** and **II** in gas phase correspond to intermolecular charge transfer (ICT) between the **4Py$^+$ECN** moiety and bromide ion (**Br$^-$**) (see Figure 7).

In all three solvents, the computed λ_{max} is blue-shifted as compared to gas and crystal structure geometry (solid-state). It is noted that λ_{max} (above 500 nm in CHCl$_3$ and above 400 nm in MeOH and AcCN solvents) corresponds to ICT between cation and anion. In precursor compounds (**Ia–IIa**), the H-1→L is a major transition occurs in gas and in CHCl$_3$ (Table S5). In this transition, there is an intramolecular charge transfer from pyridine ring to other parts of the molecule. Overall, TD-DFT results indicate that the higher absorption in **I** and **II** is due to the intermolecular charge transfer between anion and cation.

The energy gap $\Delta E_{(L-H)}$ is nearly the same (2.31 eV for **I** and 2.30 eV for **II**) and the corresponding value is slightly lower for precursor compounds (**Ia** and **IIa**). However, the energy of HOMO of **I** and its precursor compound **Ia** as well as **II** and its precursor compound **IIa** shows a significant amount of energy difference (for **I** and **Ia**:2.59 eV and for **II** and **IIa**: 3.12 eV), and similar trend is also observed in the energy of LUMO of **I–II** and **Ia–IIa** (Figure 8). The quaternization on pyridine nitrogen (N1, in salts **I–II**) makes this energy variation. Based on the above results, we conclude that the contribution of strong electron withdrawing nature of **4Py$^+$ECN** moiety made that charge is localized. The strong intra- and intermolecular interactions (between cation and anion) present in the solid-state and in solution state could be the reason for red-shifted absorption in **I** and **II** as compared to their respective precursor compounds.

Types of Intermolecular Interactions

The asymmetric units of **I–II** contain one 1-allyl-4-(1-cyano-2-(4-(dimethyl/diphenylamino)phenyl)vinyl)pyridin-1-ium cation and one bromide anion moiety (Figure 1). In both salts, the cationic molecules are self-assembled by C−H···N, C−H···π and π···π interactions whereas the cation and anion moieties are held by C−H···Br$^-$ interactions. Various molecular dimers in **I–II**, which are extracted from the respective crystal structure by using PIXEL method and interaction energies (E_{tot}) for these dimers are listed in Table 5. The interaction energy which is decom-

Figure 6. Single crystals of **I–II** and powder materials of **I–II** and **Ia–IIa**.

Table 4. Experimental and computed λ_{abs}, λ_{exp} (in nm) for I and II.

I λ_{abs} (DFT) Gas	eV	f	Major transition (%)	λ_{exp}	II λ_{abs} (DFT)	eV	f	Major transition (%)	λ_{exp}
685	1.809	0.001	H-1→L (96)		692	1.792	0.001	H-1→L (96)	
668	1.854	0.020	H-2→L (62) H→L (35)		673	1.841	0.018	H-2→L (62) H→L (34)	
619	2.002	0.073	H→L (61) H-2→L (36)		627	1.976	0.096	H→L (62) H-2→L (36)	
427	2.903	0.669	H-3→L (78) H→L+1 (20)		475	2.609	0.844	H-3→L (96)	
406	3.051	0.174	H→L+1 (26) H→L+2 (20)		416	2.981	0.046	H→L+1 (76)	
CHCl₃									
522	2.374	0.009	H-1→L (72) H→L (22)	528	546	2.270	0.211	H-1→L (58) H→L (24)	542
517	2.397	0.056	H-3→L (53) H→L (22) H-1→L (21)		543	2.284	0.251	H-1→L (40) H→L (22) H-3→L (22)	
516	2.403	0.002	H-2→L (76)		525	2.361	0.865	H→L (53) H-3→L (25) H-3→L (20)	
474	2.617	1.294	H→L (52) H-3→L (24) H-2→L (20)	315	352	3.520	0.265	H-4→L (85)	333
341	3.639	0.003	H-1→L+1 (46) H→L+1 (29)	293 271	345	3.600	0.021	H-1→L+1 (46) H-3→L+1 (27)	277
MeOH									
474	2.617	1.327	H→L (99)	510	526	2.355	1.296	H→L (99)	504
430	2.883	0.001	H-1→L (98)		447	2.773	0.002	H-1→L (97)	
426	2.909	0.007	H-3→L (63) H-2→L (35)		442	2.803	0.003	H-3→L (71) H-2→L (27)	
425	2.920	0.006	H-2→L (64) H-3→L (35)		441	2.812	0.002	H-2→L (72) H-3→L (27)	
337	3.676	0.014	H→L+2 (78)		352	3.514	0.246	H-4→L (71) H→L+1 (27)	
AcCN									
474	2.615	1.345	H→L (99)	509	527	2.352	1.301	H→L (99)	503
429	2.891	0.005	H-1→L (96)		446	2.781	0.002	H-1→L (97)	
424	2.921	0.003	H-3→L (76) H-2→L (21)		441	2.811	0.003	H-3→L (69) H-2→L (28)	
423	2.932	0.005	H-2→L (78) H-3→L (21)		440	2.820	0.002	H-2→L (71) H-3→L (28)	
337	3.678	0.014	H→L+1 (86)		352	3.513	0.245	H-4→L (72) H→L+1 (27)	
Solid									
654	1.896	0.001	H→L+1 (75)	677	749	1.654	0.010	H→L+2 (87)	
650	1.909	0.004	H-1→L+1 (76)	627	598	2.073	0.807	H-3→L (89)	615
602	2.059	0.065	H-2→L+1 (70) H-2→L+2 (21)		525	2.363	0.008	H→L+3 (99)	554
586	2.115	0.009	H-1→L+2 (80)	562	516	2.403	0.001	H→L+4 (99)	
441	2.809	1.031	H-3→L (94)	482	463	2.676	0.004	H→L+5 (99)	436
					437 456	2.719	0.002	H→L+6 (96)	
					389 377		0.200	H-4→L (85)	359

posed into Coulombic (E_{coul}), polarization (E_{pol}), dispersion (E_{dis}) and repulsion (E_{rep}) contributions summarized in Table 5. In I and II, we observed three types of interactions, (i) cation···cation, (ii) cation···anion and (iii) anion···anion interaction only in the case of II. In I, the cationic molecules are self-associated (molecular pairs **D6**--**D11**) with the help of several C–H···π, C–H···N and π···π interactions. The destabilization energy (E_{tot}) for these molecular pairs is in the range 23.3–35.0 kcal mol⁻¹.

On the other hand, the stabilizing interactions are formed between cation and anion (Br⁻) moieties with several intermolecular C–H···Br⁻ interactions (dimers **D1**--**D5** in I, and **D1**–**D6** in II) and the E_{tot} values are in the range between −77.4 and −47.0 kcal mol⁻¹ in I and −81.6 and −48.5 kcal mol⁻¹ in II. In II, the cationic molecules are self-assembled through C–H···π, C–H···N and π···π interactions (dimers **D7**–**D12**) with the destabilization interaction energy in the range of 35.2–
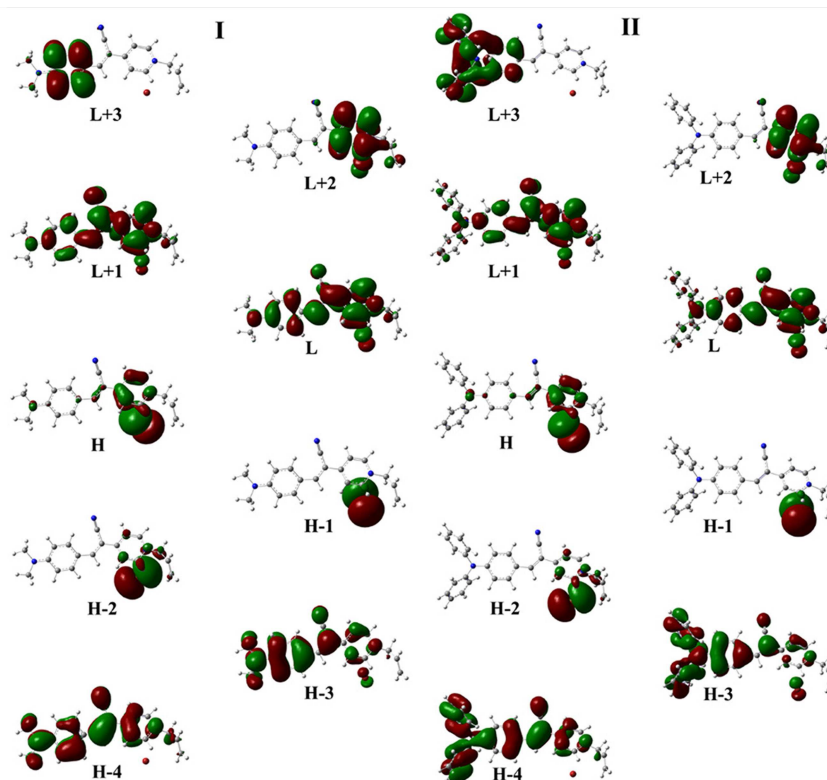
Figure 7. Electron-density distributions for the frontier molecular orbitals of **I–II** calculated at the B3YLP/6-311 + + G (d, p) level of theory in the gas phase. The orbitals plotted with isovalue = 0.02 Å^{-3}.
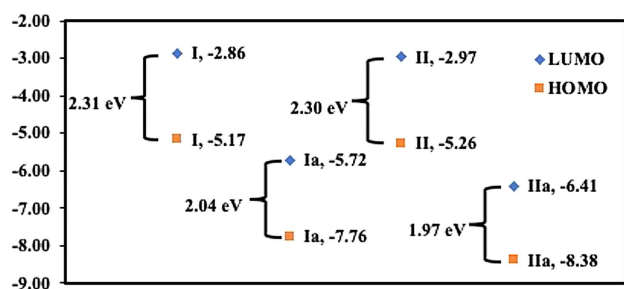

Figure 8. The molecular orbital energy levels of **I–II** and their parent compounds (**Ia–IIa**; energy in eV. This energy levels are obtained from the optimized geometry in a vacuum with B3LYP/6-311 + + G(d,p) level of theory).

11.4 kcal mol^{-1}. There is a Br$^-$···Br$^-$ interaction occurred with the distance 4.382(1) Å and there is no anion···anion contact in **I**. Further, the PIXEL interaction energies (E_{tot}) for different dimers in **I** and **II** are compared with the values of ΔE_{CP} which is calculated at the crystal geometry of the respective dimer by using the counterpoise method. The E_{tot} and ΔE_{CP} values for all dimers are comparable.

Crystal Structure of I

The crystal structure of **I** can be described as a herringbone pattern (Figure 9). Different molecular pairs identified from the
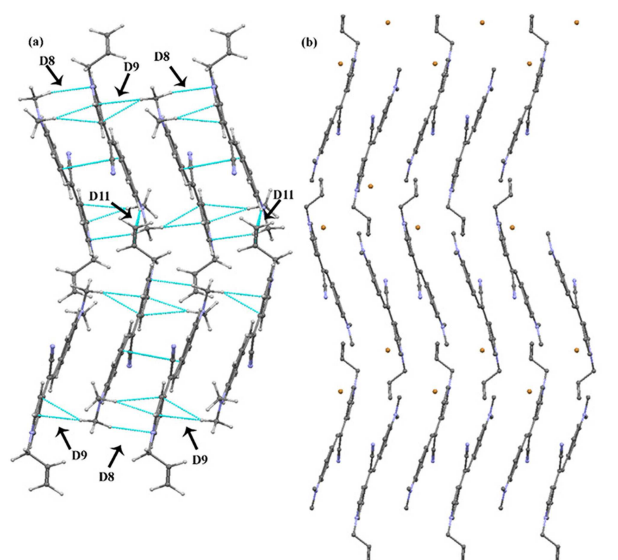

Figure 9. Overall packing arrangement of **I** in (a) cationic molecules as double arrays and (b) the cation and anion arrangement in **I**.

Table 5. Various intermolecular interactions observed in compounds I and II. (interaction energy in kcal mol^{-1}; distance is the centroid-centroid of the distance of molecules in Å; ^{a} and ^{b} are aromatic rings).

Motif/ Dimer	Possible Interactions	Geometry (Å/°) d(H···A)	d(D···A)	∠ D–H···A	Symmetry code	Distance	E_{coul}	E_{pol}	E_{disp}	E_{rep}	E_{tot}	ΔE_{CP}	HS label
Cation···Anion interactions in I													
D1	C7–H7···Br1$^-$	2.68	3.722	162	1/2+x, 1/2-y, 1/2+z	4.272	−66.9	−12.3	−4.0	5.8	−77.4	−76.28	1
	C11–H11···Br1$^-$	2.96	4.030	170									
D2	C3–H3B···Br1$^-$	2.77	3.746	150	x, y, z	7.543	−67.6	−11.2	−4.0	6.6	−76.2	−75.66	2
	C1–H1A···Br1$^-$	2.89	3.829	146									3
	C8–H8···Br1$^-$	3.09	3.888	131									
D3	C4–H4···Br1$^-$	2.62	3.579	147	1/2+x, 1/2-y, 1/2-z	7.618	−65.6	−10.6	−3.5	6.4	−73.3	−73.55	4
	C3–H3A···Br1$^-$	3.04	3.914	138									
D4	C2–H2···Br1$^-$	3.00	3.772	129	1+x, y, z	7.787	−52.5	−6.8	−2.2	2.6	−58.9	−57.04	
	C1–H1B···Br1$^-$	3.12	3.817	123									
D5	C19–H19B···Br1$^-$	2.78	3.838	165	3/2-x, 1/2+y, 3/2-z	10.335	−42.8	−5.3	−1.8	2.9	−47.0	−49.51	5
Cation···Cation interactions in I													
D6	C3–H3B··· C7(π_a)	3.16	3.937	129	1/2+x, 1/2-y, 1/2+z	10.926	41.2	−3.4	−3.7	0.8	35.0	36.65	
D7	C19–H19A···N2	2.84	3.370	110	x, y, 1+z	9.668	31.0	−1.9	−2.7	1.7	28.1	29.51	
	C16–H16···N2	2.74	3.757	156									
D8	C19-H19A···C4(π_a)	2.61	3.592	151	1-x, 1-y, +1 -z	4.639	39.0	−6.8	−22.8	17.9	27.3	32.10	6
	C18–H18C···C8 (π_a)	2.79	3.580	130									
	C10···C17 (π_b)		3.449										7
	C11···C12(π_{vinyl} ···π_b)		3.508										
D9	C18–H18A···C5 (π_a)	2.83	3.634	131	2-x, 1-y, 1-z	5.112	40.0	−4.9	−16.2	8.2	27.2	32.23	
	C9···C14 (π_{vinyl} ···π_b)		3.598										
D10	C19–H19C···C17 (π_b)	2.71	3.621	142	2-x, 1-y, 2-z	11.021	29.2	−2.6	−5.7	5.0	26.0	29.09	8
D11	C14–H14···C1 (π_{allyl})	2.60	3.447	135	3/2-x, 1/2-y, 1/2+z	13.020	26.5	−2.3	−4.4	3.4	23.3	25.17	9
Cation···Anion interactions in II													
D1	C11–H11···Br1$^-$	2.73	3.771	162	x, 1+y, z	4.492	−71.0	−15.6	−5.5	10.5	−81.6	−79.58	10
	C7–H7···Br1$^-$	2.72	3.779	167									11
	C17–H17···Br1$^-$	2.75	3.753	154									12
D2	C8–H8···Br1$^-$	2.49	3.476	152	−x, 1-y, −z	7.845	−70.4	−12.0	−3.9	8.2	−78.1	−76.20	13
D3	C4···Br1$^-$ (π_a ···Br1$^-$)		3.589		−x, −1/2+y, 1/2-z	9.274	−65.6	−9.7	−3.0	4.0	−74.3	−73.99	
D4	C4–H4···Br1$^-$	2.77	3.568	131	x, 1/2-y,1/2+z	8.532	−61.5	−9.6	−3.0	4.8	−69.3	−68.29	14
	C5–H5···Br1$^-$	3.01	3.677	121									
D5	C1–H1B···Br1$^-$	3.04	4.112	169	−x, 1/2+y, −1/2-z	12.468	−44.9	−3.6	−1.0	1.0	−48.6	−49.07	
D6	C26–H26 ···Br1$^-$	2.92	3.740	133	x, 3/2-y, 1/2+ z	6.158	−41.0	−8.0	−2.4	2.9	−48.5	−47.72	15
Cation···Cation interactions in II													
D7	C9···N2 (π_{vinyl} ···N2)		3.349		x, 3/2-y, −1/2+z	8.881	44.2	−5.0	−8.1	4.0	35.2	36.44	
	C8···C5 (π_a···π_a)		3.503										
	C2–H2···C7 (π_a)	3.09	3.859	129									
D8	C3–H3B···C11 (π_{vinyl})	2.86	3.542	121	−x, 1/2+y, 1/2-z	11.935	41.9	−5.2	−6.4	3.0	33.2	35.76	
	C3–H3A···C17 (π_b)	2.95	3.784	134									
	C3–H3B···C7 (π_a)	3.14	4.224	179									
	C1–H1A··· C13 (π_b)	3.19	3.811	117									
D9	C23–H23···H23–C23	2.35			1-x, 2-y, 1-z	9.104	22.1	−1.6	−7.8	3.6	16.2	19.47	
	C22–H22···H23–C23	2.34											
	C22–H22···C13 (π_b)	3.12	3.928	132									
D10	C14–H14···C28 (π_d)	2.54	3.566	157	x, 5/2-y, −1/2+z	7.514	22.5	−3.7	−16.7	12.7	14.8	19.96	16
	C17–H17···H25–C25	2.29											
	C29–H29···C20 (π_c)	2.73	3.616	139									17
	C20–H20···C23 (π_c)	2.83	3.478	119									
D11	C21–H21···N2	2.61	3.525		1-x, −1/2+y, 3/2-z	12.524	17.5	−0.8	−3.9	1.6	14.5	16.23	18
D12	C28–H28···C19 (π_c)	2.60	3.626	101	1-x, 3-y, 1-z	15.298	13.5	−2.4	−9.9	10.1	11.4	14.47	19
	C28–H28···H29-C29	2.37											
Anion···Anion interactions in II													
D13	Br1$^-$···Br1$^-$		4.382		−x, −y, −z	4.381	76.0	−3.2	−0.5	0.3	72.7	73.16	

crystal structure of **I** are depicted in Figure S3 along with their intermolecular interaction energies calculated from the PIXEL method.

The cationic molecules of **I** in the crystal structure are arranged as arrays which run parallel to crystallographic *b* axis (Figure 9(a)). In each array, molecules are interlinked in a head (*N,N*-dimethyl phenyl side)-to-tail (allyl group) manner by an intermolecular C–H···π interaction (**D11**, E_{tot}: 23.3 kcal mol^{-1}). The molecules in one array interact with molecules in the adjacent array through π···π and C–H···π interactions together (**D8**, E_{tot}: 27.3 kcal mol^{-1}). For the π···π interaction, ring B is stacked against the cyano group (C10≡N2) and the *N,N*-

dimethyl group acts as a donor and ring A as an acceptor for the C–H···π interaction. The motif **D8** makes the molecules formed as double arrays. The adjacent double arrays are further interconnected by C–H···π interaction (**D9**, E_{tot}: 27.2 kcal mol^{-1}, Figure 9(a)) to form the herringbone architecture generated by cationic molecules of **I**. The bromide anions are in the vicinity of allyl group and the anions are placed inside the double arrays in the crystal. Except for ring B, other functional units (allyl, pyridine, acrylonitrile and *N, N*-dimethyl) are involved in the intermolecular C–H···Br$^-$ interactions. A detailed discussion on the arrangement of ion pairs is given in the separate section. Further, the allyl group is involved in the intermolecular C–H···π interactions (C3–H3B··· π_a in **D6**; E_{tot}: 35.0 kcal mol^{-1} and C14–H14···π_{allyl} in **D11**; E_{tot}: 23.3 kcal mol^{-1}) and the latter interaction plays an important to like the molecules as arrays as mentioned earlier. Furthermore, the cyano group is involved in three-centered intermolecular C–H···N interactions as an acceptor. These interactions (**D7**, E_{tot}: 28.1 kcal mol^{-1}) link the neighbouring molecules into a chain which runs parallel to *c* axis (Figure 10).
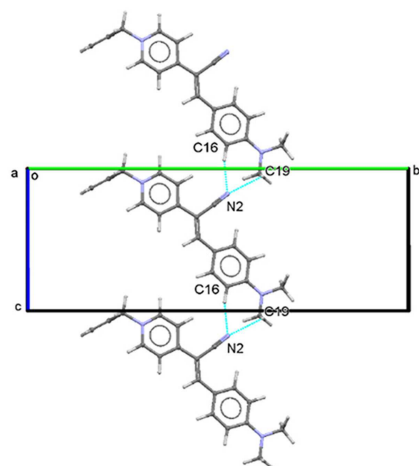

Figure 10. Part of the crystal packing of **I** showing the C16–H16···N2 and C19–H19 A···N2 interactions which link the molecules into a chain.

Crystal Structure of II

The crystal structure of **II** is presented in Figure 11. Various molecular pairs identified from the crystal structure of **II** are illustrated in Figure S4, along with their intermolecular interaction energies calculated from the PIXEL method. The crystal structure of **II** is completely different from that of the crystal structure of **I**. All the functional units (allyl, pyridine, acrylonitrile, *N, N*-diphenyl and phenyl) of **II** participate in the intermolecular C–H···Br$^-$ interactions.

The overall structure can be described as a compact double helical structure in which quarternized pyridine ring placed outside the helical backbone. Both helical chains are formed by intermolecular C–H···π interaction (**D10**, E_{tot}: 14.8 kcal mol^{-1}). One of the *N, N*-diphenyl rings in one helical chain is in a
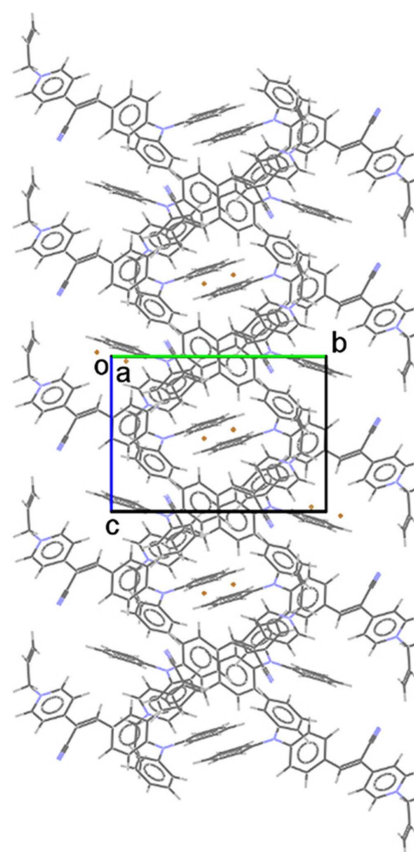

Figure 11. The double helical packing arrangement of **II**.

displaced stacking with another *N, N*-diphenyl ring comes from the neighbouring helical chain at the center. This arrangement is stabilized by C–H···π (**D12**, E_{tot}: 11.4 kcal mol^{-1}). The anions are located within the displaced stacking of *N,N*-diphenyl rings and *N, N*-diphenyl rings are also located on the helical grooves. The C–H···N interactions in **D11** (E_{tot}: 14.5 kcal mol^{-1}) link the neighbouring molecules into a zigzag chain which runs parallel to *b* axis (Figure S5). Further, the allyl group has also participated in the intermolecular C–H···π interactions with ring B and acrylonitrile moiety of the cationic molecule (**D8**, E_{tot}: 33.2 kcal mol^{-1}) and it also involved in stabilizing interaction (C–H···Br$^-$) with anions (**D5** with E_{tot}: −48.6 kcal mol^{-1}). In addition, the substituted *N, N*-diphenyl groups are engaged in several C–H···π interactions (**D9**, **D10** and **D12**) and an intermolecular C–H···Br$^-$ interaction (**D6**, E_{tot}: −48.5 kcal mol^{-1}). It is noted that the atom C4 of the pyridine ring interacts with an anion (C···Br$^-$ interaction; motif **D3**; E_{tot}:-74.3 kcal mol^{-1}) and its existence was confirmed by the QTAIM analysis. The E_{HB} value for C4···Br$^-$ contact is 1.10 kcal mol^{-1}.

To confirm the existence of various noncovalent interactions observed in different molecular pairs, the topological properties were computed for the intermolecular interactions at the bond critical points in **I** and **II** (Table S6, ESI) and molecular graphs for these dimers are illustrated in (Figures, S6 and S7, ESI). The stabilizing energies (E_{HB}) calculated by QTAIM approach for these interactions are in the range of 0.94 (motif **D4**) –

2.31(motif **D1**) kcal mol^{-1} in **I** and 0.98 (motif **D5**) – 3.88 (motif **D2**) kcal mol^{-1} in **II**. The corresponding values are found to be in the range of 0.5(**D6**) – 1.54 (**D11**) kcal mol^{-1} for C—H···π interactions in **I** (0.5 (**D7**) – 1.89 (**D10**) kcal mol^{-1} in **II**). The E_{HB} value for the C—H···N is calculated to be 0.98 (**D7** in **I**) kcal mol^{-1} and 1.28 (**D11** in **II**) kcal mol^{-1}. This result suggests that some of the C—H···π and C—H···N interactions energies are slightly stronger in **II**. In addition, there are four H···H interactions observed in different molecular pairs (E_{HB}:0.8 kcal mol^{-1} in **D9** and 1.2 kcal mol^{-1} in **D12**) and these interactions provide additional stabilization to the crystal structure along with other types of interactions in **II**. It should be noted there is no H···H type of interaction observed in **I**.

To understand the relationship between the topological parameters (particularly, electron density (ρ) and the Laplacian electron density ($\nabla^2\rho$) and bond path distance (R_{ij}) at the BCP's between the interacting atoms. It is noted that the H···Br$^-$ interactions in **I** and **II** display the trend of exponential decay (with R^2 > 0.98) in the magnitude of electron density (ρ) and the Laplacian electron density ($\nabla^2\rho$) with the increasing length of bond path (Figure S8, ESI).

Arrangement of Ion Pairs in the Crystal Structures of I and II

Figure 12 describes the arrangement of ions (the centroid is taken for cationic molecule) in the crystal structures of both salts. The bromide ions in **I** arranged as double ions in a zigzag manner which runs parallel to the *a* axis and the inter-ionic distance within double ions is 6.096 Å and the adjacent double ions are separated by 7.554 Å. Similarly, the cationic molecules are also arranged as double cations with the inter-ionic distance being 4.655 Å and the adjacent double ions are placed at a distance of 5.125 Å. Overall, alternate cationic and anionic zigzag chains are arranged in the crystal structure. However, the arrangement of cations and anions are completely different in **II** as compared to the crystal structure of **I**. The anions are formed as double arrays and these arrays are sandwiched between the cationic arrays. The distance between two anionic arrays is

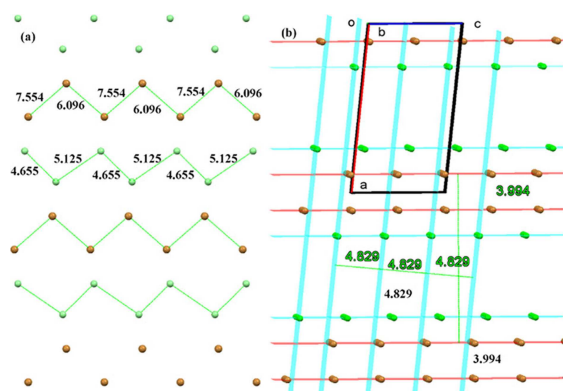**Figure 12.** The arrangement of cations and anions in the crystal structure of (a) **I** and (b) **II**. Cations (green) and anions (brown) are shown as small green spheres. (interionic distance in Å).

3.994 Å which supports for the formation of a destabilizing Br$^-$ ···Br$^-$ contact.

Lattice Energies

The overall lattice energies of **I** and **II** and their precursors are partitioned into their Coulombic (E_{coul}), polarization (E_{pol}), dispersion (E_{dis}) and repulsion (E_{rep}) contributions summarized in Table 6. From Table 6, compound **II** is more stable

Table 6. The lattice energies of I–II and Ia–IIa in kcal mol^{-1}.

Compound	E_{coul}	E_{pol}	E_{disp}	E_{rep}	E_{tot}
I	−5.3	−7.4	−28.0	23.9	−16.9
Ia (TENMIK01)[a]	−5.8	−6.2	−39.4	13.1	−37.4
TENMIK[a]	−5.8	−6.1	−37.3	13.3	−35.8
II	−15.9	−12.9	−35.1	30.4	−84.2
IIa (AWEGEQ)[a]	−5.6	−7.1	−50.0	17.2	−45.5

[a]CCDC reference code for the precursor compounds

(−84.2 kcal mol^{-1}) than **I** (−16.9 kcal mol^{-1}). The larger difference on the lattice energy between **I** and **II** is might be due to the presence of *N, N*-diphenyl group in **II** which helps to pack the molecules more compact. The lattice energy difference is in good agreement with the melting points of **I** and **II** (∼20 °C higher in **II**). In the case of **II**, a notable increase of Coulombic and polarization energies (the contribution of Coulombic energy is 3 fold higher and polarization energy is approximately 2 fold higher as compared to **I**) is observed. The contribution of repulsive energies is also more pronounced in **II** than other structures due to compact crystal packing.

NBO Analysis

In order to learn the origin of intermolecular charge transfer process between cation and anion moieties in **I** and **II**, we performed NBO analysis for various dimeric pairs formed by intermolecular C—H···Br$^-$ interactions. The second order perturbation energies for different donor-acceptor NBOs are summarized in Table 7. The results suggest that the interactions between the lone pair orbitals of the anion and the CH groups (anti-bonding) of the pyridine ring are observed to give the strongest stabilization energy in both **I** and **II**. We note that the charge transfer [LP(4) Br→BD*(C8—H8)] is even stronger in **II**. The allyl group is also involved in the intermolecular charge transfer process with the moderate stabilization energy. Moreover, all the CH groups of allyl moiety is participated in the charge transfer in **I**, while C2—H and C3—H groups in **II** are not involved in the charge transfer because the allyl group adopts different conformation as compared to **I**. The interaction between anti-bonding orbital of C11—H11 group and LP(4) Br anion is more stronger (3.92 kcal mol^{-1}) in **II**. The corresponding interaction is slightly weaker (1.58 kcal mol^{-1}) in **I**.

Table 7. Selected cation-anion charge transfer process in I–II and its corresponding second order perturbation energy ($E^{(2)}$ in kcal mol^{-1}).

Dimer	Compound I			Compound II		
	Donor NBO	Aceptor NBO	$E^{(2)}$	Donor NBO	Aceptor NBO	$E^{(2)}$
D1	LP (4) Br	BD*(1) C7—H7	5.64	LP (4) Br	BD*(1) C7—H7	4.15
	LP (4) Br	BD*(1) C11—H11	1.58	LP (4) Br	BD*(1) C11—H11	3.92
				LP (3) Br	BD*(1) C17—H17	2.71
D2	LP (4) Br	BD*(1) C3—H3B	3.34	LP (4) Br	BD*(1) C8—H8	10.53
	LP (3) Br	BD*(1) C1—H1A	1.31			
D3	LP (4) Br	BD*(1) C4—H4	6.19	LP (4) Br	BD*(2) C4=C5	2.20
	LP (4) Br	BD*(1) C3—H3A	0.57			
D4	LP (4) Br	BD*(1) C2—H2	1.14	LP (4) Br	BD*(1) C4—H4	3.57
	LP (4) Br	BD*(1) C1—H1B	0.43	LP (2) Br	BD*(1) C5—H5	0.73
D5	LP (4) Br	BD*(1) C19—H19B	4.18	LP (3) Br	BD*(1) C1—H1B	1.22
D6				LP (3) Br	BD*(1) C26—H26	1.35
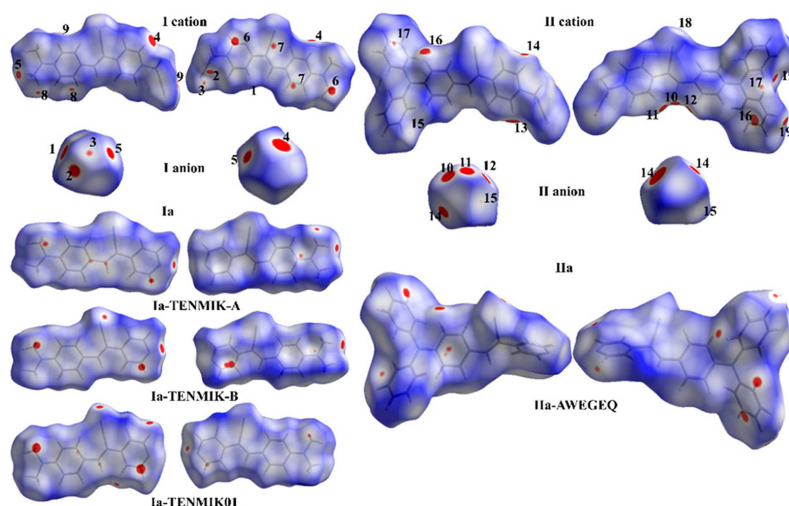
Figure 13. Views of the Hirshfeld surface mapped with d_{norm} in two different orientations for **I** and **II** with their precursor compounds (**Ia** for **TENMIK-A**; **TENMIK-B** and **TENMIK01**; **IIa** for **AWEGEQ**). The significant contacts are labelled. To refer Table 5 for the more details about the interactions.

Hirshfeld Surface Analysis

It is well known that the HS analysis is a useful visualization tool for the analysis of intermolecular interactions in the crystal packing and FP analysis is also used to quantify the contribution of various intermolecular contacts present in the crystal structures. The HS mapped with d_{norm} was obtained for **I–II** and their precursor molecules (Figure 13). The close contacts observed in these structures are labelled (see Table 5). Nine intermolecular interactions (label 1–9) are visible on the HS of **I** whereas there are 10 intermolecular close contacts (label 10–19) seen on the HS of **II**.

A close examination of the FP generated for **I–II** and their precursor molecules indicating that the intermolecular H···H interactions are predominant (Figure 14 and 15). In **II**, the intermolecular C···H/H···C contacts are contributing 30.1% to the total HS area. This contact is reduced to 20.2% in **I** and this reduction is compensated by intermolecular C···C, N···H and H···Br interactions contacts. This is clearly supporting the presence of more C···H/H···C interactions in **II** and presence of π···π interactions in **I**. It should be emphasized that the H···N is decreased in **II** when compared to its precursor molecule (AWEGEQ) and other contacts are comparable. It is to be noted

that the relative contribution of all types of contacts observed in **I** is altered as compared to its precursor (different forms) molecule.

3. Conclusions

The variation in the optical properties due to the formation of the respective quaternary salts and due to the charge transfer (CT). It was also due to the strong effect on the structure of the electron acceptor group of the quarternized salts. In the solid-state absorption spectra, there was a broadening of the peak in the salts and this broadening was absent in precursor compounds. This observation had clearly highlighted the effect of quarternization. Further, the variation of bond lengths of selected bonds observed in the crystal structures was supported for the existence of a strong push-pull character of **I–II**. Due to the strong push-pull nature of **I** and **II**, there was a red-shift ($<$ 100 nm) observed in the absorption because of the presence of **4Py$^+$ECN** moiety. The charge transfer occurred between cation and anion was confirmed through DFT calculation. The arrangement of cations and anions are completely different in the crystal structures of **I** (herringbone) and **II** (double helical).
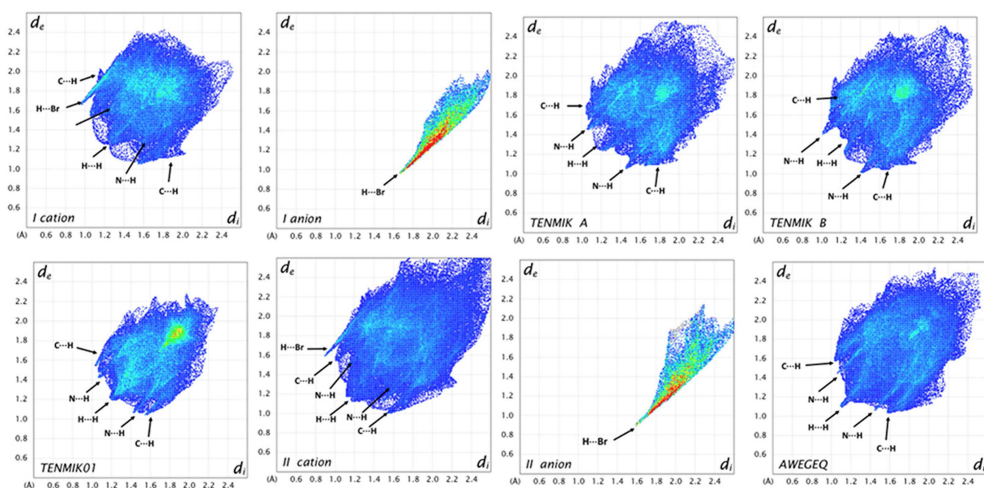
Figure 14. 2D Finger print (FP) plots for **I–II** along with their precursor compounds. The important contacts are labelled.
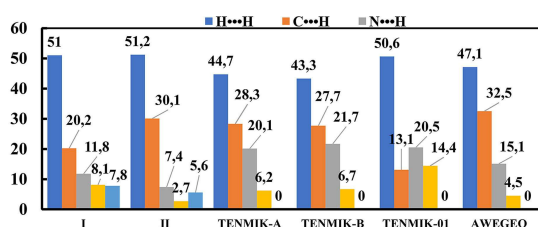

Figure 15. Relative contributions of various intermolecular contacts in **I** and **II** along with their precursor compounds.

Differences in the solid-state structure which led to alter the optical properties. Further, the crystal structures, supramolecular architectures and packing motifs of **I–II** were also analyzed through different computational tools such as PIXEL, HS and QTAIM calculations. In both salts, the cationic moiety was found to be destabilized by C—H···N, C—H···π and π···π interactions whereas the cationic and anionic species were predominantly stabilized by C—H···Br⁻ interactions in both crystal structures. NBO analysis suggested that there are strong intermolecular charge transfers between pyridine group and anion. The existence of charge transfer between cation and anion groups provided a strong bathochromic shift in **I–II** when compared with their precursor compounds **Ia–IIa**.

Experimental Section

Synthesis and Crystallization

General Experimental Procedure for the Synthesis of Salts I–II

As shown in Scheme 5, the compound (Z)-3-(4-(dimethylamino) phenyl)-2-(pyridin-4-yl)-acrylonitrile (**Ia**) and (Z)-3-(4-(diphenylami-no)phenyl)-2-(pyridin-4-yl)acrylonitrile (**IIa**) were synthesized from 4-N,N-substituted aminobenzldehyde (**Ib–IIb**) and 4-(cyanomethyl) pyridin-1-ium chloride(**2**) as reported earlier.[18b,d, e] The mixture of **Ia** or **IIa** (1 mmol) and allyl bromide (**3**, 1.1 mmol) in 25 mL of acetone were refluxed for 12 h. Upon completion of the reaction, the

reaction mixture was cooldown to room temperature and the salts (**I–II**) were settled as precipitates. The precipitates were collected by the vacuum filtration and washed with acetone. The products (**I–II**) were dried under vacuum. Both salts(**I–II**) were purified by recrystallization from acetone and methanol (1 : 1 v/v) mixture.

Synthesis of (Z)-1-allyl-4-(1-cyano-2-(4-(dimethylamino) phenyl)-vinyl) Pyridin-1-ium Bromide (I)

The reaction was carried out as mentioned in the general procedure using (Z)-3-(4-(dimethylamino)phenyl)-2-(pyridin-4-yl) acrylonitrile (**Ia**, 250 mg, 1 mmol) and allyl bromide (**3**, 135 mg, 1.1 mmol), conditions: refluxed for 12 h. The compound **I** was obtained as purple colour solid (300 mg, 80% yield). The compound **I** was purified by the recrystallization from methanol and acetone (1 : 1 v/v) mixture. m.p 198–200 °C. IR (KBr) 3005, 2675, 2597, 2208, 1638, 1610, 1556, 1521, 1450, 1370, 1231, 1198, 1160, 850, 531 cm⁻¹; ^{1}H NMR (500 MHz, DMSO-d$_6$): δ 8.90 (d, J = 7 Hz, 2H), 8.54 (s, 1H), 8.27 (d, J = 7.5 Hz, 2H), 8.09 (d, J = 9 Hz, 2H), 6.93 (d, J = 9.5 Hz, 1H), 6.21–6.13 (m,1H), 5.5–5.38 (m,2H), 3.25 (s, 6H); ^{13}C (125 MHz, DMSO-d6) δ 19.4, 60.7, 61.7, 65.9, 100.7, 112.6, 116.8, 123.0, 124.6, 130.3, 130.7, 150.0, 155.5, 158.4, 170.7, 172.5. Mass (Direct, EI⁺ method): 290 (M⁺), 265, 249(100%), 221.

Synthesis of (Z)-1-allyl-4-(1-cyano-2-(4-(diphenylamino) phenyl)- Vinyl)pyridin-1-ium Bromide (II)

The reaction was carried out as mentioned in the general procedure using (Z)-3-(4-(diphenylamino)phenyl)-2-(pyridin-4-yl) acrylonitrile (**IIa**, 100 mg, 0.26 mmol) and allyl bromide(**3**, 35 mg, 0.29 mmol), conditions: refluxed for 12 h. The compound **II** was obtained as deep brown colour solid (105 mg, 82% yield). The product was purified by the recrystallization from methanol and acetone (1 : 1 v/v) mixture. m.p 219–220 °C. IR (KBr) 3174, 3089, 3057, 2963, 2927, 2781, 2598, 2204, 1588, 1486, 1410, 1069, 1012 cm⁻¹; ^{1}H NMR (500 MHz, CDCl$_3$): δ 9.09 (d, 2H, J = 10 Hz), 8.54 (s, 1H), 8.40 (d, 2H, J = 10 Hz), 8.13 (d, 2H, J = 10 Hz), 7.41–7.37 (m, 4H), 7.26–7.24(m, 2H), 7.22–7.21 (m, 4H), 6.97 (d, 2H, J = 10 Hz), 6.17–6.09 (m,1H), 5.64–5.54(m, 4H); ^{13}C NMR (125 MHz, CDCl$_3$) δ 153.4, 152.1, 151.6, 145.1, 143.9, 134.5, 130.0, 129.9, 126.8, 126.1, 124.1, 123.9, 122.5, 118.6, 117.1, 98.0, 62.5. Mass (Direct, EI⁺ method): 414 (M⁺), 373 (100%), 345, 294, 268, 241.

Single Crystal X-Ray Diffraction (SCXRD)

The intensities were measured at 110(2) K using a SuperNova diffractometer (equipped with Atlas detector) with Cu $K\alpha$ radiation ($\lambda = 1.54178$ Å) for **I** and Mo $K\alpha$ radiation ($\lambda = 0.71073$ Å) for **II**. The program CrysAlisPro (Versions 1.171.36.32 Agilent Technologies, 2013 or 1.171.39.29c, Rigaku OD, 2017) was used to refine the cell dimensions and for data reduction. The structures were solved with the program SHELXS-97[22] and were refined on F^2 with SHELXL-2014/7.[23] An analytical numeric absorption correction using a multifaceted crystal model or a numerical absorption correction based on Gaussian integration over a multifaceted crystal model was applied using CrysAlisPro. The temperature of the data collection was controlled using the system Cryojet (manufactured by Oxford Instruments). The H atoms were placed at calculated positions using the instructions AFIX 23, AFIX 43, AFIX 93 or AFIX 137 with isotropic displacement parameters having values 1.2 or 1.5 Ueq of the attached C atoms. The crystal data refinement parameters are summarized in Table 1. Displacement ellipsoidal plots and crystal packing figures were made using the programs PLATON[24] and MERCURY,[25] respectively.

Hirshfeld Surface Analysis, and PIXEL Energy Calculation

The Hirshfeld surfaces (HS) analysis[20a–c,e, 26] and the decomposed two-dimensional fingerprint plots (FP)[27] was used to quantify the contribution of different intermolecular interactions existing in the crystal structure and to understand the nature of intermolecular interactions. The HS and FP were generated using the program CrystalExplorer17.[28] Further, the intermolecular interaction energies (E_{tot}) for different molecular pairs of **I–II** were calculated using the PIXEL method (in the CLP computer program package version 12.5.2014).[29] Based on the E_{tot} values, the selected molecular pairs were considered for further analysis. The total lattice energies of the title salts (**I–II**) and their precursor compounds (**Ia–IIa**) were also computed using the PIXEL method. The C—H bond lengths were adjusted to typical neutron diffraction values (C—H = 1.089 Å) before the HS and PIXEL calculations. For PIXEL calculations, the electron density of the molecules was obtained at MP2/6-31G** level of theory using Gaussian09 for all the molecules in the current study.

Quantum Chemical Calculations

All the quantum chemical calculations were performed with the Gaussian 09 program package.[30] For structural optimization, the respective crystal structure geometry was used for **I–II** and **Ia–IIa** as a starting model. These structures were fully optimized using M05-2X[31]/cc-PVTZ level of theory with the incorporation of Grimme's D3 dispersion corrections.[32] The selection of M05-2X functional and basis set has been made based on our earlier studies.[33] The vibrational frequency was calculated for the optimized structures in the gas phase in order to ascertain the global minima on the potential energy surface and was found to have no negative frequencies. Further, the interaction energies (ΔE_{CP}) for the various molecular dimers at their crystal geometry were calculated at M05-2X/cc-pVTZ level of theory. The ΔE_{CP} was corrected for basis set superposition error (BSSE)[34] using the counterpoise method. To explore the solvent (chloroform, methanol and acetonitrile) influence, we used the conductor-like polarizable continuum model (CPCM)[35] for all solution-phase structural optimization. Time-dependent DFT (TD-DFT)[36] approach was used to calculate the absorption properties with B3LYP/6-311++G(d, p) level of theory. Furthermore, we performed natural bond orbital (NBO) analysis to characterize the nature of charge transfer between the cation and anion moieties in **I** and **II**.

Analysis of Topological Parameters (QTAIM Calculations)

We performed topological analysis on the selected dimers by using the AIMALL package (T. A. Keith, AIMALL, version 16.05.18; TK Gristmill Software, Overland Park KS, USA, 2013). For this purpose, the DFT calculation (with the density = current keyword) for the selected molecular pairs at their crystal geometry was performed at the MP2/6-31G** level of theory. The dissociation energies for different intermolecular interactions at the bond critical point (BCP) were estimated using two empirical approaches as proposed earlier,[37] (i) D.E.^{V}(int) = $-0.5V_b$ (a.u.)[37] (ii) D.E.^{G}(int) = $0.429G_b$ (a.u.) Where D.E.(int) is the dissociation energy of the interaction (interaction energy (E_{HB}) = $-D.E.$(int));[37] V_b and G_b are the local potential and kinetic energy density at the bond critical points (BCP's), respectively.

UV-Vis Absorbance

The absorbance spectra were measured using a spectrometer SD2000 (Ocean Optics, Dunedin, FL) with a DT 1000 CE light source (Analytical Instrument Systems, Inc., Flemington, NJ). For powder samples, the absorption spectra were measured using the Spectrometer Cary 300 (Agilent) in the mode the diffuse reflectance.

Supporting Information

Supporting information for this article is given via a link at the end of the document.(bond length and torsion angle comparison of **I–II** and their precursor structures (**Ia–IIa**); Experimental and computed λ_{abs} (in nm) for **Ia** and **IIa**; Different interacting dimers in the crystal structure of **I** and **II** along with the interaction energies in kcal mol^{-1} and selected topology parameters and molecular graph with BCP's for an individual dimers in **I** and **II**.)

Conflict of Interest

The authors declare that there is no conflict of interest.

[1] F. W. B. van Leeuwen, J. C. H. Hardwick, A. R. van Erkel, *Radiology* **2015**, *276*, 12–29.

[2] a) P. Bosch, F. Catalina, T. Corrales, C. Peinado, *Chem. Eur. J.* **2005**, *11*, 4314–4325; b) J. Pączkowski, *Polimery* **2005**, *50*, 520–529; c) R. P. Haugland, Molecular probes: Handbook of fluorescent probes and research chemicals, Interchim (Molecular Probes Inc, PO Box 22010 Eugene, OR 97402–0414, USA,) **1992–1994**.

[3] A. W. Bajorek, M. Pietrzak, *Chemik* **2011**, *65*, 255–260.

[4] A. W. Bajorek, K. Trzebiatowska, B. Jędrzejewska, M. Pietrzak, R. Gawinecki, J. Pączkowski, *J. Fluoresc.* **2004**, *14*, 295–307.

[5] a) S. Wróblewski, K. Trzebiatowska, B. Jędrzejewska, M. Pietrzak, R. Gawinecki, J. Pączkowski, *J. Chem. Soc. Perkin Trans. 2,* **1999**, 1909–1917; b) A. Bajorek, J. Pączkowski, *Polimery* **2007**, *52*, 556–561.

[6] P. Fromherz, A. Heilemann, *J. Phys. Chem.* **1992**, *96*, 6864–6866.

[7] B. Strehmel, H. Seifert, W. Rettig, *J. Phys. Chem. B* **1997**, *101*, 2232–2243.

[8] C. Y. Y. Yu, W. J. Zhang, R. T. K. Kwok, C. W. T. Leung, J. W. Y. Lam, B. Z. Tang, *J. Mater. Chem. B* **2016**, *4*, 2614–2619.

[9] C. Y. Yu, H. Xu, S. Ji, R. T. Kwok, J. W. Lam, X. Li, S. Krishnan, D. Ding, B. Z. Tang, *Adv. Mater.* **2017**, *29*, 1606167.

[10] a) J. Yong Lee, K. S. Kim, B. Jin Mhin, *J. Chem. Phys.* **2001**, *115*, 9484–9489; b) L. R. Dalton, *J. Phys. Condens. Matter* **2003**, *15*, R897; c) M. Kivala, F. Diederich, *Acc. Chem. Res.* **2009**, *42*, 235–248.

[11] a) J. C. May, I. Biaggio, F. Bures, F. Diederich, *Appl. Phys. Lett.* **2007**, *90*, 251106; b) M. G. Kuzyk, *J. Mater. Chem.* **2009**, *19*, 7444–7465.

[12] M. Kivala, F. Mitzel, C. Boudon, J. P. Gisselbrecht, P. Seiler, M. Gross, F. Diederich, *Chem. Asian J.* **2006**, *1*, 479–489.

[13] a) E. Kleinpeter, S. Klod, W.-D. Rudorf, *J. Org. Chem.* **2004**, *69*, 4317–4329; b) F. Bureš, W. B. Schweizer, C. Boudon, J. P. Gisselbrecht, M. Gross, F. Diederich, *Eur. J. Org. Chem.* **2008**, *2008*, 994–1004; c) J. Rotzler, D. Vonlanthen, A. Barsella, A. Boeglin, A. Fort, M. Mayor, *Eur. J. Org. Chem.* **2010**, *2010*, 1096–1110; d) M. Ababneh-Khasawneh, B. E. Fortier-McGill, M. E. Occhionorelli, A. D. Bain, *J. Phys. Chem. A* **2011**, *115*, 7531–7537.

[14] a) G. Archetti, A. Abbotto, R. Wortmann, *Chem. Eur. J.* **2006**, *12*, 7151–7160; b) E. L. Spitler, L. D. Shirtcliff, M. M. Haley, *J. Org. Chem.* **2007**, *72*, 86–96; c) M. Becuwe, D. Landy, F. Delattre, F. Cazier, S. Fourmentin, *Sensors* **2008**, *8*; d) A. S. Andersson, L. Kerndrup, A. Ø. Madsen, K. Kilså, M. B. Nielsen, P. R. L. Porta, I. Biaggio, *J. Org. Chem.* **2009**, *74*, 375–382; e) N. Hebbar, Y. Ramondenc, G. Plé, G. Dupas, N. Plé, *Tetrahedron* **2009**, *65*, 4190–4200; f) M. Klikar, P. le Poul, A. Růžička, O. Pytela, A. Barsella, K. D. Dorkenoo, F. Robin-le Guen, F. Bureš, S. Achelle, *J. Org. Chem.* **2017**, *82*, 9435–9451; g) N. F. Montcada, L. Cabau, C. V. Kumar, W. Cambarau, E. Palomares, *Org. Electron.* **2015**, *20*, 15–23; h) J. Kulhánek, F. Bureš, *Beilstein J. Org. Chem.* **2012**, *8*, 25–49.

[15] F. Bureš, *RSC Adv.* **2014**, *4*, 58826–58851.

[16] A. Forni, R. Destro, *Chem. Eur. J.* **2003**, *9*, 5528–5537.

[17] M. J. Percino, M. Cerón, P. Ceballos, G. Soriano-Moro, O. Rodríguez, V. M. Chapela, M. E. Castro, J. Bonilla-Cruz, M. A. Siegler, *CrystEngComm* **2016**, *18*, 7554–7572.

[18] a) M. J. Percino, M. Cerón, P. Venkatesan, P. Ceballos, A. Bañuelos, O. Rodríguez, M. A. Siegler, F. Robles, V. M. Chapela, G. Soriano-Moro, E. Pérez-Gutiérrez, J. Bonilla-Cruz, S. Thamotharan, *Cryst. Growth Des.* **2017**, *17*, 1679–1694; b) M. J. Percino, M. Cerón, O. Rodríguez, G. Soriano-Moro, V. Chapela, M. Siegler, E. Pérez-Gutiérrez, *Molecules* **2016**, *21*, 389; c) M. J. Percino, M. Ceron, P. Ceballos, G. Soriano-Moro, M. E. Castro, V. M. Chapela, J. Bonilla-Cruz, M. Reyes-Reyes, R. Lopez-Sandoval, M. A. Siegler, *J. Mol. Struct.* **2014**, *1078*, 74–82; d) M. J. Percino, M. Ceron, P. Ceballos, G. Soriano-Moro, O. Rodriguez, V. M. Chapela, M. E. Castro, J. Bonilla-Cruz, M. A. Siegler, *CrystEngComm* **2016**, *18*, 7554–7572; e) M. J. Percino, V. M. Chapela, M. Cerón, G. Soriano-Moro, M. E. Castro, F. J. Melendez, *J. Mol. Struct.* **2013**, *1034*, 238–248.

[19] a) A. Gavezzotti, *J. Phys. Chem. B* **2002**, *106*, 4145–4154; b) A. Gavezzotti, *J. Phys. Chem. B* **2003**, *107*, 2344–2353; c) A. Gavezzotti, *New J. Chem.* **2011**, *35*, 1360–1368.

[20] a) J. J. McKinnon, D. Jayatilaka, M. A. Spackman, *Chem. Commun.* **2007**, 3814-3816; b) J. J. McKinnon, M. A. Spackman, A. S. Mitchell, *Acta Crystallogr. Sect. B* **2004**, *60*, 627–668; c) J. J. McKinnon, S. A. Mitchell, M. Spackman, *Chem. Eur. J.* **1998**, *4*, 2136–2141; d) M. A. Spackman, P. G. Byrom, *Chem. Phys. Lett.* **1997**, *267*, 215–220; e) M. A. Spackman, D. Jayatilaka, *CrystEngComm* **2009**, *11*, 19–32.

[21] a) R. F. W. Bader, *Chem. Rev.* **1991**, *91*, 893–928; b) R. F. W. Bader, *Atoms in Molecules: A Quantum Theory*, Clarendon Press, (ISBN: 9780198558651.) **1994**.

[22] G. Sheldrick, *Acta Crystallogr. Sect. A* **2008**, *64*, 112–122.

[23] a) G. Sheldrick, *Acta Crystallogr. Sect. C* **2015**, *71*, 3–8; b) G. Sheldrick, *Acta Crystallogr. Sect. A* **2015**, *71*, 3–8.

[24] A. L. Spek, *J. Appl. Crystallogr.* **2003**, *36*, 7–13.

[25] a) C. F. Macrae, P. R. Edgington, P. McCabe, E. Pidcock, G. P. Shields, R. Taylor, M. Towler, J. van de Streek, *J. Appl. Crystallogr.* **2006**, *39*, 453–457; b) C. F. Macrae, I. J. Bruno, J. A. Chisholm, P. R. Edgington, P. McCabe, E. Pidcock, L. Rodriguez-Monge, R. Taylor, J. van de Streek, P. A. Wood, *J. Appl. Crystallogr.* **2008**, *41*, 466–470.

[26] M. A. Spackman, J. J. McKinnon, D. Jayatilaka, *CrystEngComm* **2008**, *10*, 377–388.

[27] M. A. Spackman, J. J. McKinnon, *CrystEngComm* **2002**, *4*, 378–392.

[28] M. J. Turner, J. J. McKinnon, S. K. Wolff, D. J. Grimwood, P. R. Spackman, M. A. Spackman, CrystalExplorer17, **2017**, *University of Western Australia*. http://hirshfeldsurface.net.

[29] A. Gavezzotti, *Mol. Phys.* **2008**, *106*, 1473–1485.

[30] M. J. Frisch, G. W. Trucks, H. B. Schlegel, G. E. Scuseria, M. A. Robb, J. R. Cheeseman, G. Scalmani, V. Barone, B. Mennucci, G. A. Petersson, H. Nakatsuji, M. Caricato, X. Li, H. P. Hratchian, A. F. Izmaylov, J. Bloino, G. Zheng, J. L. Sonnenberg, M. Hada, M. Ehara, K. Toyota, R. Fukuda, J. Hasegawa, M. Ishida, T. Nakajima, Y. Honda, O. Kitao, H. Nakai, T. Vreven, J. A. Montgomery, J. E. Peralta, F. Ogliaro, M. Bearpark, J. J. Heyd, E. Brothers, K. N. Kudin, V. N. Staroverov, R. Kobayashi, J. Normand, K. Raghavachari, A. Rendell, J. C. Burant, S. S. Iyengar, J. Tomasi, M. Cossi, N. Rega, J. M. Millam, M. Klene, J. E. Knox, J. B. Cross, V. Bakken, C. Adamo, J. Jaramillo, R. Gomperts, R. E. Stratmann, O. Yazyev, A. J. Austin, R. Cammi, C. Pomelli, J. W. Ochterski, R. L. Martin, K. Morokuma, V. G. Zakrzewski, G. A. Voth, P. Salvador, J. J. Dannenberg, S. Dapprich, A. D. Daniels, Farkas, J. B. Foresman, J. V. Ortiz, J. Cioslowski, D. J. Fox, Gaussian 09, Wallingford CT **2009**.

[31] a) Y. Zhao, N. E. Schultz, D. G. Truhlar, *J. Chem. Theory Comput.* **2006**, *2*, 364–382; b) E. G. Hohenstein, S. T. Chill, C. D. Sherrill, *J. Chem. Theory Comput.* **2008**, *4*, 1996–2000.

[32] S. Grimme, J. Antony, S. Ehrlich, H. Krieg, *J. Chem. Phys.* **2010**, *132*, 154104.

[33] a) P. Venkatesan, M. Ceron, S. Thamotharan, F. Robles, M. J. Percino, *CrystEngComm* **2018**, *20*, 2681–2697; b) M. Udayakumar, K. Jagatheeswaran, S. S. Ganesan, N. S. Venkataramanan, S. M. Kumar, K. Byrappa, S. Thamotharan, *J. Mol. Struct.* **2017**, *1133*, 510–518; c) P. Venkatesan, S. Thamotharan, A. Ilangovan, H. Liang, T. Sundius, *Spectrochim. Acta Part A* **2016**, *153*, 625–636; d) P. Venkatesan, S. Thamotharan, R. G. Kumar, A. Ilangovan, *CrystEngComm* **2015**, *17*, 904–915; e) S. Thamotharan, J. Kothandapani, S. Selva Ganesan, N. S. Venkataramanan, S. Madan Kumar, K. Byrappa, J. Percino, F. Robles, *J. Chem. Sci.* **2018**, *130*, 20.

[34] S. F. Boys, F. Bernardi, *Mol. Phys.* **1970**, *19*, 553–566.

[35] a) S. Miertuš, E. Scrocco, J. Tomasi, *Chem. Phys.* **1981**, *55*, 117–129; b) J. Tomasi, B. Mennucci, R. Cammi, *Chem. Rev.* **2005**, *105*, 2999–3094.

[36] W. Kohn, L. J. Sham, *Phys. Rev.* **1965**, *140*, A1133-A1138.

[37] E. Espinosa, E. Molins, C. Lecomte, *Chem. Phys. Lett.* **1998**, *285*, 170–173.

[38] a) A. Ilangovan, P. Venkatesan, M. Sundararaman, R. Rajesh Kumar, *Med. Chem. Res.* **2012**, *21*, 694–702; b) T. Seethalakshmi, P. Venkatesan, R. J. Butcher, M. Nallu, P. Kaliannan, *Acta Crystallogr. Sect. E* **2006**, *62*, O4730-O4731; c) T. Seethalakshmi, P. Venkatesan, M. Nallu, D. E. Lynch, S. Thamotharan, *Acta Crystallogr. Sect. E* **2013**, o884; d) M. Sundararaman, R. Rajesh Kumar, P. Venkatesan, A. Ilangovan, *J. Med. Microbiol.* **2013**, *62*, 241–248; e) P. Venkatesan, V. Rajakannan, S. Thamotharan, *Acta Crystallogr. Sect. E* **2014**, 580–583.

[39] a) B. Carlotti, G. Consiglio, F. Elisei, C. G. Fortuna, U. Mazzucato, A. Spalletti, *J. Phys. Chem. A* **2014**, *118*, 3580–3592; b) B. Carlotti, G. Consiglio, F. Elisei, C. G. Fortuna, U. Mazzucato, A. Spalletti, *J. Phys. Chem. A* **2014**, *118*, 7782–7787; c) A. Cesaretti, B. Carlotti, G. Consiglio, T. Del Giacco, A. Spalletti, F. Elisei, *J. Phys. Chem. B* **2015**, *119*, 6658–6667; d) B. Carlotti, A. Cesaretti, C. G. Fortuna, A. Spalletti, F. Elisei, *Phys. Chem. Chem. Phys.* **2015**, *17*, 1877–1882; e) B. Carlotti, E. Benassi, A. Cesaretti, C. G. Fortuna, A. Spalletti, V. Barone, F. Elisei, *Phys. Chem. Chem. Phys.* **2015**, *17*, 20981–20989.

[40] B. Carlotti, E. Benassi, A. Spalletti, C. G. Fortuna, F. Elisei, V. Barone, *Phys. Chem. Chem. Phys.* **2014**, *16*, 13984–13994.

[41] H. Görner, *J. Photochem. Photobiol. A* **2011**, *218*, 199–203.

[42] H. Güsten, D. Schulte-Frohlinde, *Z. Naturforsch. B Chem. Sci.* **1979**, *34*, 1556–1566.